PCCP

ROYAL SOCIETY OF CHEMISTRY

PAPER

View Article Online
View Journal | View Issue

Check for updates

Cite this: *Phys. Chem. Chem. Phys.*, 2023, **25**, 25361

Electron ionization induced fragmentation pathways of trichloroanisole†

Mónica Mendes, [a] Daniel Bou-Debes, [b] Samuel Eden, [b] Nenad Bundaleski, [a] Orlando M. N. D. Teodoro, [a] Lucas M. Cornetta*[c] and Filipe Ferreira da Silva *[a]

Received 2nd May 2023,
Accepted 29th August 2023

DOI: 10.1039/d3cp02019c

rsc.li/pccp

Trichloroanisole (TCA) is one of the most significant contaminants in cork stoppers. The presence of TCA leads to an unpleasant odor known as "cork taint", resulting in high economic losses for the cork and wine industries. Hence, the detection, quantification, and characterization of TCA are essential to address this concern. The present study investigates the electron-driven fragmentation pathways of TCA through electron ionization mass spectrometry as a function of electron energy (0–100 eV), and the results are supported by theoretical characterization of ionization potentials, dissociation thresholds, and electron ionization cross sections. The appearance energies of ten cations were measured, including the first experimental evaluation of the molecule's ionization energy at 8.8 ± 0.3 eV, in excellent agreement with the calculations (8.83 eV). For lower energies, around 20 eV, the parent cation accounted for more than 60% of the total ion signal, followed by its demethylated fragment. Taken together, these ion signals could be used as fingerprints of TCA in industrial quality control by low-energy electron ionization mass spectrometry. Fifty other fragments have been identified at higher electron energies, revealing the very rich fragmentation pattern of TCA.

Published on 29 August 2023. Downloaded on 11/29/2025 8:01:51 PM.

Introduction

Trichloroanisole ($C_7Cl_3H_5O$), particularly the isomer 2,4,6-trichloroanisole (TCA), belongs to the family of haloanisoles, and is a major compound in wine contamination. The presence of TCA in wine and cork stoppers leads to sensory defects, mostly characterized by an unpleasant musty, mouldy or earthy odour which is known as "cork taint".[1–3] Its formation can result from the microbiological methylation of chlorophenols through the process of *O*-methylation of 2,4,6-trichlorophenol (2,4,6-TCP) by filamentous fungi[3–7] or from reaction pathways associated with other fungi such as *Penicillium* species.[1] The molecule has a low organoleptic threshold value ($\sim$4 ng L^{-1}) and it is estimated that 70% of tainted cork is contaminated by TCA.[8–10] The impact of TCA contamination on the cork and wine producers is substantial, since 1–5% of total wine bottles may present defective cork stoppers which motivated the use of metal and polymer closures for wine bottling.[11,12] The analysis and characterization of haloanisoles can be achieved through analytical procedures using accurate and highly sensitive instrumentations, this is therefore an important area of development for the industry. Several analytical methods have been proposed to determine the concentration of the main compounds responsible for tainted wine.[2,9,13–19] Currently, quantification of TCA for quality control is done by soaking a few stoppers out of many thousand for 24 hours followed by solid phase microextraction gas chromatography (SPME-GC) analysis.[12,20–22] Concentrations as low as $\approx$1 ng L^{-1} of TCA in the soak are relevant for wine consumers. However, these surveys are time-consuming and only allow a limited number of cork stoppers to be analyzed. Thus, in the past decade the cork industry started searching for remediation technologies as well as analytical instruments for fast online detection.

Asfandiarov *et al.*[5] have investigated 2,4,6-TCA and 2,4,6-tribromoanisole through dissociative electron attachment and electron transmission spectroscopy. TCA was also studied using ion mobility spectrometry and different chemical ionization schemes were presented for various produced ions.[3,13] A novel method was recently reported for the online detection of TCA based on chemical ionization mass spectrometry (CI-MS) without the need to use chromatography.[23] Peres *et al.*[24] suggested an analysis through cyclic voltammetry (CV) which yields good results when compared with standard gas chromatography mass spectrometry (GS-MS) methods, and provides a fast, user-friendly and low-cost alternative for quality control. Alternative systems in the literature to quantify TCA in cork samples

[a] *CEFITEC, Department of Physics, Nova School of Sciences and Technology, Caparica P-2829-516, Portugal. E-mail: f.ferreiradasilva@fct.unl.pt*
[b] *School of Physical Sciences, The Open University, Walton Hall, Milton Keynes, MK7 6AA, UK*
[c] *Instituto de Física Gleb Wataghin, Universidade Estadual de Campinas, Campinas, São Paulo, Brazil. E-mail: lucascor@unicamp.br*

† Electronic supplementary information (ESI) available. See DOI: https://doi.org/10.1039/d3cp02019c

Published on 29 August 2023. Downloaded on 11/29/2025 8:01:51 PM.

include biosensors based on screen printed electrodes,[25] electrochemical displacement immunosensors[26] and cellular biosensors systems based on the bioelectric recognition.[27] The novel instrument based on CI-MS is so fast and sensitive that it can detect TCA released from corks at a concentration below 1 ng L^{-1} in 3 s. In fact, mass spectrometry is among the techniques with the lowest LOD (limit of detection) and can also be very fast. However, one of the constraints of this technique is the presence of many volatile species not only released by cork but also present in industrial air. To overcome this, a mass resolution of about 4000 is required.

In the present study, the application of electron ionization mass spectrometry for TCA monitoring and identification is discussed. Despite producing ion fragmentation, electron ionization is a powerful technique for identifying molecules. For this purpose, it is valuable to know how the intensity of ion fragments varies with the electron energy. We aim to contribute to a faster TCA detection technique that allows a high number of corks to be analysed reliably at a low cost. Positive ion formation upon low energy electron interaction with gas-phase TCA is characterized by using a trochoidal electron monochromator (TEM) coupled with an orthogonal reflectron time-of-flight mass spectrometer (OReTOFMS). The ionization efficiency curves for the most intense cations are presented, as well as the respective threshold energies. The energy dependence of ion formation is also evaluated for energies between 20 and 100 eV through branching ratios calculations. Quantum chemical calculations were used to help the identification of the observed fragments. The focus of the present work is not the identification of TCA in contaminated air in a production environment but the characterization of its ionization potentials, dissociation thresholds and electron ionization branching ratios. This study aims to tackle the problem of TCA in cork stoppers by using electron impact ionization and mass spectrometry.

Materials and methods

The presented results have been obtained in a crossed electron-molecule beam apparatus, described in detail elsewhere.[28] In brief, an electron beam is generated by a trochoidal electron monochromator, with an estimated energy resolution of 190 meV. The formed ions are extracted towards the reflectron time of flight mass spectrometer, by a low electric field ($\sim$1 V cm^{-1}). In the mass spectrometer, the ions are guided to the reflectron by a pulsed extracting voltage of -380 V, impinging the microchannel plate detector. The working pressure in the collision chamber was 5×10^{-5} Pa and the base pressure was 1×10^{-6} Pa. Mass spectra were recorded from $\sim$0 eV to 100 eV in steps of 10 meV. For the threshold energy determination, a Wannier fitting[29] procedure was applied as explained in detail by Pereira-da-Silva *et al.*[28] The energy scale was calibrated by using the Ar^+ threshold energy 15.763 eV, determined by Weitzel *et al.*[30] through ZEKE-PEPICO (zero kinetic energy photoelectrons photoions coincidence).

The TCA sample was purchased from Sigma-Aldrich with a minimum purity of 99% and used as delivered. The TCA sample was degassed through repeated freeze–pump–thaw cycles, and introduced in the chamber via a side entrance, connected directly to the collision region of the monochromator. The measurements were performed at room temperature ($\sim$21 °C).

Theoretical calculations were conducted in order to support and analyse the measurements. Electron ionization of the TCA molecule was described within Binary–Encounter–Bethe (BEB) model.[31] The binding and kinetic energies of the molecular orbitals were obtained using the outer valence Green's function (OVGF) electron propagator theory,[32] together with the 6-311++G(2df,2p) basis set. The appearance energies are understood to be the lowest energies to enable reactions. From a theoretical perspective, that quantity can be investigated by inspection of the thermodynamic thresholds, characterizations of transition states and further aspects of potential energy surfaces. In a general sense, calculating thermodynamic thresholds is one of the best approaches, as they provide a lower bound for the appearance energy. Since tunnelling effects make it possible for a reaction to happen with energies between the threshold energy and the energy barrier, characterizing transition states is more relevant for determining reaction rates rather than appearance energies. In this work, the thermodynamic thresholds for the formation of the most relevant cationic fragments were determined using the composite G4(MP2) methodology,[33] which is a high level procedure with benchmark quality. All calculations were performed using the Gaussian16 package.[34]

The search for transition states for some of the reactions were conducted, but no significant differences in relation to the thresholds, were found. In fact, the potential energy surface of the lowest-lying cation is such that some fragmentation pathways follow Morse-like dynamics along the reaction coordinate, without a transition state. That seems to be the case for the fragment m/z 195, which is related to the O–CH_3 bond break. Inspection of the potential energy surface along the C–O stretching indicates an asymptotic Morse-like behaviour with different dissociative limits, depending on the angle between CH_3 group and the ring plane (see Fig. S3, ESI†)

Results

Fig. 1 shows the mass spectrum of TCA recorded at 70 eV incident electron kinetic energy. The counterpart of the radical methyl group (m/z 195) represents the most intense signal, followed by the formation of the parent cation (m/z 210) and the counterpart of the radical methoxy group (m/z 167). Table 1 summarizes the observed fragments with their relative intensities in the 70 eV mass spectrum.

Energy scans for the ten most abundant fragments have been recorded (Fig. 2) for determining appearance energies (AEs). In addition, these energy scans characterise the quantum yield near the threshold representing the appearance energies for each reaction. As described in Section 2, a Wannier

 This journal is © the Owner Societies 2023

Published on 29 August 2023. Downloaded on 11/29/2025 8:01:51 PM.

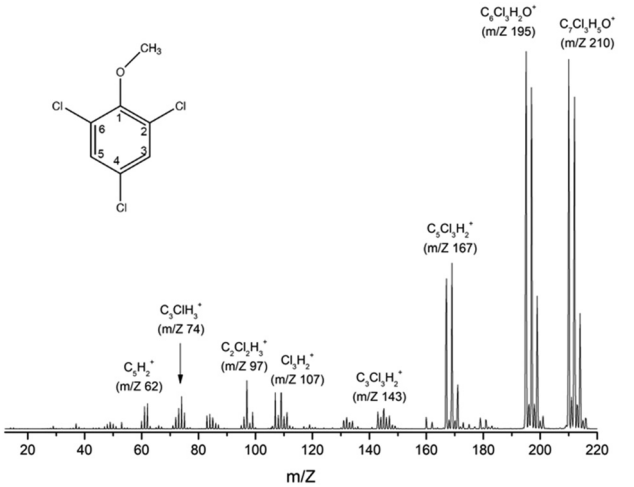

Fig. 1 TCA ($C_7Cl_3H_5O$) electron ionization mass spectrum recorded at 70 eV incident electron energy. The geometry of TCA is illustrated schematically in the top-left corner.

Table 1 List of cationic fragments with relative intensities >5% under electron ionization at 70 eV incident electron energy

Cation	*m*/*z*	Relative intensity (%)
$C_5H^+/C_2ClH_2^+$	61	5.9
$C_5H_2^+$	62	6.7
$C_3ClH_2^+$	73	5.5
$C_3ClH_3^+$	74	8.5
$C_2Cl_2H^+$	97	12.8
$C_3Cl_2H^+$	107	9.5
$C_3Cl_2H^+$ isotope	109	9.5
$C_3Cl_3H_2^+$	143	5.1
$C_5Cl_3H_2^+$	167	39.8
$C_5Cl_3H_2^+$ isotope	169	44.0
$C_5Cl_3H_2^+$ isotope	171	11.6
$[TCA\text{-}CH_3]^+$	195	100
$[TCA\text{-}CH_3]^+$ isotope	196	6.5
$[TCA\text{-}CH_3]^+$ isotope	197	90.5
$[TCA\text{-}CH_3]^+$ isotope	198	6.6
$[TCA\text{-}CH_3]^+$ isotope	199	35.2
TCA^+	210	97.9
TCA^+ isotope	211	8.4
TCA^+ isotope	212	88.0
TCA^+ isotope	213	6.4
TCA^+ isotope	214	30.6

method[29] was applied to determine the AEs. Uncertainties have been determined by combining the maximum deviation of the average of three different measurements with the statistical uncertainty of the fitting. Table 2 compares the experimental appearance energies with theoretical calculated values showing a good agreement between the two data sets; the uncertainly limits of the experimental values mostly overlap with the theoretical values (with the exception of the relatively weakly produced ions at *m*/*z* 73, 74, and 97).

Discussion

The experimental ionization potential has been determined at 8.8 ± 0.3 eV being in good agreement with the theoretical value obtained at 8.83 eV. Fig. S1 (ESI†) illustrates the 20 first orbitals

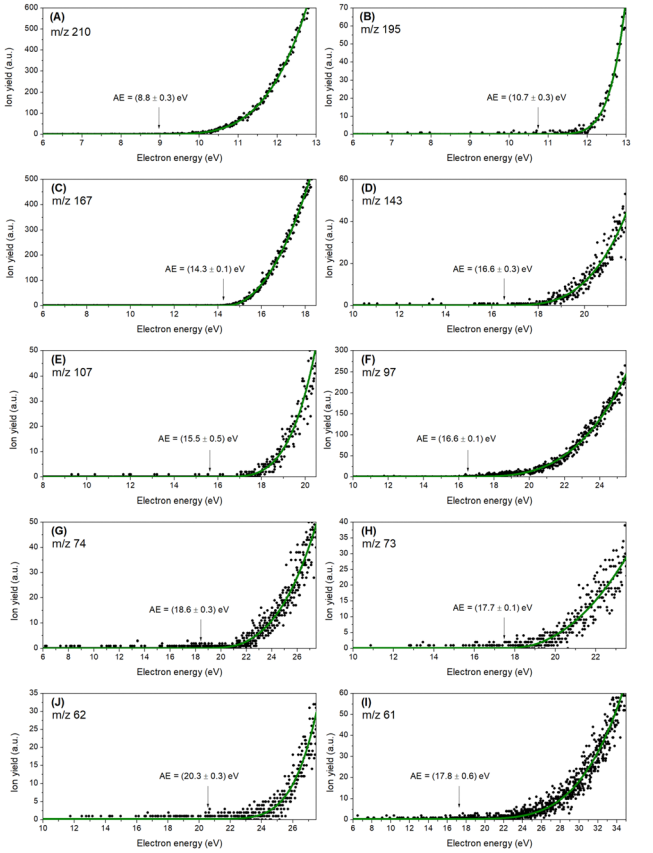

Fig. 2 Experimental thresholds for the ten most abundant cations (A-I), decreasing in *m*/*z*. The black dots represent the experimental data, and the green line represents the Wannier-type fitting function. The values in parentheses correspond to the experimental thresholds with the respective statistical uncertainties. Wannier-type fitting parameters are summarized in Table S2 (ESI†).

Table 2 Experimental and theoretical threshold energies for the ten most intense cations

Cation	*m*/*z*	Experimental (eV)	Theoretical (eV)
TCA^+	210	8.8 ± 0.3	8.83
$[TCA\text{-}CH_3]^+$	195	10.7 ± 0.3	10.50
$C_5Cl_3H_2^+$	167	14.3 ± 0.1	14.40
$C_3Cl_3H_2^+$	143	16.6 ± 0.3	16.89
$C_3Cl_2H^+$	107	15.5 ± 0.5	14.72
$C_2Cl_2H^+$	97	16.6 ± 0.1	17.21
$C_3ClH_3^+$	74	18.6 ± 0.3	17.90
$C_3ClH_2^+$	73	17.7 ± 0.1	17.21
$C_5H_2^+$	62	20.3 ± 0.3	20.03
$C_5H^+/C_2ClH_2^+$	61	17.8 ± 0.6	17.79

(HOMO to HOMO−19) along with the corresponding ionization potentials (increasing from 8.84 eV to 17.90 eV). The total ionization cross section for each molecular orbital is shown individually in the ESI† (Fig. S2). The total cross section maximum is 82.84 a_0^2 and occurs at 81.63 eV. The most intense fragment ion (*m*/*z* 195), corresponding to the loss of CH_3 radical from the TCA cation, has an experimental threshold energy of 10.7 ± 0.3 eV, quite close to the theoretical value of 10.50 eV.

Published on 29 August 2023. Downloaded on 11/29/2025 8:01:51 PM.

The lower-mass fragment ions with more than 5% relative intensity are associated with ring opening reactions. The threshold for the formation of $C_5Cl_3H_2^+$ (m/z 167) was experimentally determined at 14.3 ± 0.1 eV in agreement with theoretical value at 14.40 eV. This fragment corresponds to the loss of the radical methoxy group with an additional carbon atom ($COCH_3$). Further fragmentation leading to lighter cations such as $C_3Cl_3H_2^+$ (m/z 143), $C_3Cl_2H^+$ (m/z 107), $C_2Cl_2H^+$ (m/z 97), $C_3ClH_3^+$ (m/z 74), and $C_3ClH_2^+$ (m/z 73) involve more complex internal rearrangements. For those fragment cations, the experimental energy thresholds have been determined as 16.6 ± 0.3 eV, 15.5 ± 0.5 eV, 16.6 ± 0.1 eV, 18.7 ± 0.3 eV, 17.7 ± 0.1 eV, respectively. The calculated theoretical values for $C_3Cl_3H_2^+$ (m/z 143), $C_3Cl_2H^+$ (m/z 107), $C_2Cl_2H^+$ (m/z 97), were found at 16.89 eV, 14.72 eV, 17.21 eV, respectively, in agreement with the experiment, and are individually discussed in the following paragraphs.

The relation between the m/z 73 and m/z 74 cations can be inferred by considering the relative intensities of their peaks in Fig. 1 and also their appearance energies. Their experimental appearance energies differ by 0.9 ± 0.5 eV, which is too great to attribute to isotopic effects. Moreover, by analyzing peak intensities, we find that the isotopic contribution is negligible. We conclude that the features arise from a combination of both isotopic distributions and hydrogen elimination channels. Dissociation thresholds were calculated for the formation of $C_3ClH_3^+$ (m/z 74) and $C_3ClH_2^+$ (m/z 73), with obtained values ranging from 12.9 eV to 15 eV for the different analyzed conformers. These are below the experimental appearance energies of 18.6 ± 0.3 eV and 17.7 ± 0.1 eV, respectively. Even though such disagreement could in principle be explained by Cl elimination in the counterpart, the fact that the m/z 74 fragment has the higher appearance energy points to an orbital selectivity instead. In fact, the HOMO−18 and HOMO−19 have IPs of 17.21 eV and 17.90 eV, respectively, and are in a good agreement with the experimental values. Hence, we suggest that the process leading to the $C_3ClH_2^+$ (m/z 73) cation may involve an electron ejection from HOMO−18, whereas the process leading to the $C_3ClH_3^+$ (m/z 74) cation is related to an electron ejection from the HOMO−19 orbital. It is worth pointing out that the higher IPs lie above 21 eV, bigger than the observed appearance energies. Since the calculated thresholds for the m/z 73 and m/z 74 fragments correspond to IPs, it is reasonable to expect a slight discrepancy between the theory and experiment, due to the intrinsic error of the OVGF methodology for higher IPs. Additionally, this could be combined-with an underestimate of the experimental errors of these channels.

A closer inspection at the fragment m/z 62 reveals a large group of isomer possibilities, therefore a good description of the energetics is useful to characterize the favoured reaction path. The $C_5H_2^+$ fragment can have at least five stable structures,[35] while its neutral counterpart $C_2H_3Cl_3O$ can present itself as trichloroethanol or as ether-chloromethyl-dichloromethyl (Reaction a). The calculated dissociation thresholds for the proposed reaction possibilities were found between 13.45 eV and 16.79 eV, the latter still being 3.29 eV below the experimental appearance energy. Since the dissociation of the C–Cl bond is about 3.6 eV, we consider for this channel the possibility of a three-product reaction, with the formation of two neutral radical fragments $C_2H_3Cl_2$ and Cl (Reaction b). This reaction has a threshold of 20.03 eV, in very good agreement with the experimental value, and this is the value assigned as the theoretical prediction for the fragment 62 m/z in Table 2. The reaction is notable due to the elimination of neutral Cl, which is not observed in the other studied channels.

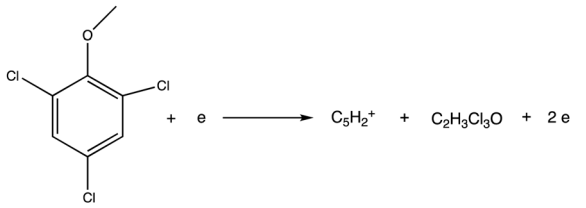

Reaction a. Direct dissociation leading to m/z 62.

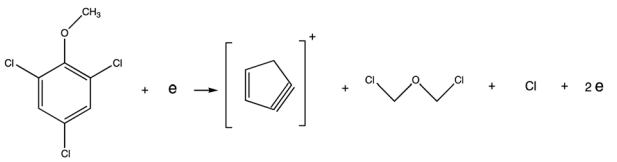

Reaction b. Dissociation leading to m/z 62, with two neutral counterparts.

Finally, the fragment m/z 61 was investigated in a similar way as the fragment m/z 62. The cation was assigned to have the molecular formula C_5H^+, where the stable linear structure was considered. In this case, the formation of C_5H^+ counts with the formation of the neutral counterpart $C_2H_3Cl_3O$ plus a hydrogen elimination. The threshold for this reaction was calculated at 17.79 eV, against the experimental value of 17.8 ± 0.6 eV.

Apart from the referred fragments, up to 50 fragments with relative intensity <5% were identified. These fragments are listed in Table S1 (ESI†) and a tentative assignment is indicated.

Fig. 3 summarizes the branching ratio behaviour as a function of the incident electron energy, between 20 and 100 eV in steps of 10 eV. Each branching ratio is determined by dividing the area of the specific cation peak by the sum of all the peak areas. The figure shows significantly enhanced branching ratios for the formation of the parent cation together with the cation formed by the loss of methyl group, in the low energy regime (below 40 eV). Indeed at 20 eV electron ionization, parent cation formation corresponds to >60% of the total ion signal. The prevalence of the parent cation and demethylated parent cation formation in the low energy regime, may be a useful tool for TCA identification. This behaviour represented by the presence of two strong peaks could be used as a fingerprint of TCA.

 This journal is © the Owner Societies 2023

Published on 29 August 2023. Downloaded on 11/29/2025 8:01:51 PM.

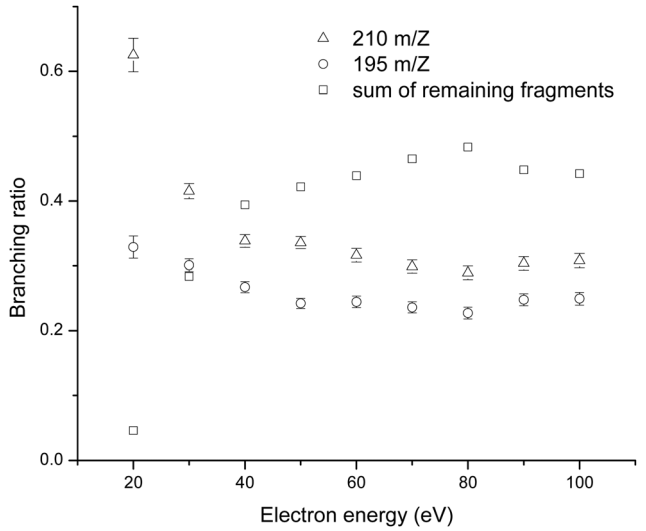

Fig. 3 Electron energy dependency of the branching ratios for *m*/*z* 210, parent cation (triangles), *m*/*z* 195, demethylated parent cation (circles), and the sum of all remaining fragments (squares), from 20 to 100 eV, in 10 eV steps.

Conclusions

In this article, we have investigated positive ion formation upon electron interactions with TCA, an important contaminant molecule for the wine industry. The ionization energy has been experimentally determined at 8.8 ± 0.3 eV, in very good agreement with the obtained theoretical value of 8.83 eV. Threshold energies for the fragment cations with relative intensities above 5% have been determined and compared with the obtained theoretical values. Generally, the two sets of data are in excellent agreement. The theoretical calculations support some complex fragmentation reactions. For the *m*/*z* 62 cation, for example, the calculations suggest the formation of two neutral radical counterparts. Additionally, a detailed analysis of the mass spectrum led to the identification of 50 fragment ions.

By analyzing the branching ratios as a function of the electron energy, it was observed that fragmentation becomes richer with the increase of the electron energy. For energies above 40 eV the fragmentation channels are dominated by lighter species, in contrast to energies around 20 eV, where the mass spectrum is dominated by the parent cation and the demethylated cation fragment. The parent cation formation in this energy range accounts for more than 60% of the total ion signal. The energy dependence revealed by the present results suggests a useful procedure for identifying TCA, by means of electron ionization. The presence of only two dominant ions in mass spectrum at low electron energies around 20 eV, accompanied with a very weak contribution of smaller fragments, represents a fingerprint of the TCA molecule.

Author contributions

Conceptualization, F. F. S., N. B. and O. M. N. D. T.; methodology and data acquisition, M. M., and D. B. D; theoretical calculations L. C.; writing – original draft preparation, M. M., L. C. and F. F. S.; writing – review and editing, S. E. F. F.S. and L. C.; all authors have read and agreed to the published version of the manuscript.

Conflicts of interest

There are no conflicts to declare.

Acknowledgements

The authors acknowledge the Portuguese National Funding Agency FCT-MCTES through the research grant number UID/FIS/00068/2020 (CEFITEC). LMC acknowledges the FAPESP funding agency under process nr. 2020/04822-9. DBD acknowledges the Open University for funding his studentship as well as the Sir John and Lady Mason Academic Trust for supporting his contributions to experiments in Lisbon.

References

1 R. Jung and V. Schaefer, *Managing Wine Quality: Volume 2: Oenology and Wine Quality*, Woodhead Publishing Limited, 2021, pp. 477–507.
2 J. I. Cacho, J. Nicolás, P. Viñas, N. Campillo and M. Hernández-Córdoba, Direct sample introduction-gas chromatography-mass spectrometry for the determination of haloanisole compounds in cork stoppers, *J. Chromatogr. A*, 2016, **1475**, 74–79.
3 Z. Lichvanová, V. Ilbeigi, M. Sabo, M. Tabrizchi and Š. Matejčík, Using corona discharge-ion mobility spectrometry for detection of 2,4,6-Trichloroanisole, *Talanta*, 2014, **127**, 239–243.
4 M. L. Álvarez-Rodríguez, L. López-Ocaña, J. M. López-Coronado, E. Rodríguez, M. J. Martínez, G. Larriba and J. J. R. Coque, Cork taint of wines: Role of the filamentous fungi isolated from cork in the formation of 2,4,6-trichloroanisole by O methylation of 2,4,6-trichlorophenol, *Appl. Environ. Microbiol.*, 2002, **68**, 5860–5869.
5 N. L. Asfandiarov, M. V. Muftakhov, S. A. Pshenichnyuk, P. Papp, M. Danko, M. Lacko, J. Blaško, S. Matejčik and A. Modelli, Dissociative electron attachment to 2,4,6-trichloroanisole and 2,4,6-tribromoanisole molecules, *J. Chem. Phys.*, 2017, **147**, 234302.
6 L. Maggi, A. Zalacain, V. Mazzoleni, G. L. Alonso and M. R. Salinas, Comparison of stir bar sorptive extraction and solid-phase microextraction to determine halophenols and haloanisoles by gas chromatography-ion trap tandem mass spectrometry, *Talanta*, 2008, **75**, 753–759.
7 A. Tarasov, M. Cabral, C. Loisel, P. Lopes, C. Schuessler and R. Jung, *Grapes and Wine*, 2022.
8 M. A. Sefton and R. F. Simpson, Compounds causing cork taint and the factors affecting their transfer from natural cork closures to wine – A review, *Aust. J. Grape Wine Res.*, 2005, **11**, 226–240.

Published on 29 August 2023. Downloaded on 11/29/2025 8:01:51 PM.

9 S. Boutou and P. Chatonnet, Rapid headspace solid-phase microextraction/gas chromatographic/mass spectrometric assay for the quantitative determination of some of the main odorants causing off-flavours in wine, *J. Chromatogr. A*, 2007, **1141**, 1–9.
10 A. Peña-Neira, B. Fernández De Simón, M. C. García-Vallejo, T. Hernández, E. Cadahía and J. A. Suarez, Presence of cork-taint responsible compounds in wines and their cork stoppers, *Eur. Food Res. Technol.*, 2000, **211**, 257–261.
11 A. Tarasov, D. Rauhut and R. Jung, ''Cork taint'' responsible compounds. Determination of haloanisoles and halophenols in cork matrix: A review, *Talanta*, 2017, **175**, 82–92.
12 M. Careri, V. Mazzoleni, M. Musci and R. Molteni, Study of electron beam irradiation effects on 2,4,6-trichloroanisole as a contaminant of cork by gas chromatography-mass spectrometry, *Chromatographia*, 2001, **53**, 553–557.
13 Z. Karpas, A. V. Guamán, D. Calvo, A. Pardo and S. Marco, The potential of ion mobility spectrometry (IMS) for detection of 2,4,6-trichloroanisole (2,4,6-TCA) in wine, *Talanta*, 2012, **39**, 200–205.
14 T. J. Evans, C. E. Butzke and S. E. Ebeler, Analysis of 2,4,6-trichloroanisole in wines using solid-phase microextraction coupled to gas chromatography-mass spectrometry, *J. Chromatogr. A*, 1997, **786**, 293–298.
15 S. H. Patil, K. Banerjee, S. C. Utture, A. R. Fontana, J. C. Altamirano, D. P. Oulkar, S. S. Wagh, S. Dasgupta, S. B. Patil, M. R. Jadhav, B. R. Ugare, P. G. Adsule and M. B. Deshmukh, Development and validation of a simple analytical method for the determination of 2,4,6-trichloroanisole in wine by GC-MS, *Food Chem.*, 2011, **124**, 1734–1740.
16 M. Riu, M. Mestres, O. Busto and J. Guasch, Determination of 2,4,6-trichloroanisole in wines by headspace solid-phase microextraction and gas chromatography-electron-capture detection, *J. Chromatogr. A*, 2002, **977**, 1–8.
17 R. Juanola, D. Subirà, V. Salvadó, J. A. Garcia Regueiro and E. Anticó, Evaluation of an extraction method in the determination of the 2,4,6-trichloroanisole content of tainted cork, *J. Chromatogr. A*, 2002, **953**, 207–214.
18 J. L. Gómez-Ariza, T. García-Barrera and F. Lorenzo, Optimisation of a two-dimensional on-line coupling for the determination of anisoles in wine using ECD and ICP-MS after SPME-GC separation, *J. Anal. At. Spectrom.*, 2005, **20**, 883–888.
19 S. Monteiro, N. Bundaleski, A. Malheiro, M. Cabral and O. M. N. D. Teodoro, Cross Contamination of 2,4,6-Trichloroanisole in Cork Stoppers, *J. Agric. Food Chem.*, 2022, **70**, 6747–6754.
20 Cork Stoppers – Determination of Releasable 2,4,6-Trichloroanisole (TCA), ISO 207522017, 2017.
21 J. Huang, L. Alquier, J. P. Kaisa, G. Reed, T. Gilmor and G. Vas, 2, 4, 6-Trichlorophenol in Various Drug Products Using Stir Bar Sorptive Extraction and Gas Chromatography – Tandem Mass Spectrometry Detection, *J. Chromatogr. A*, 2012, **1262**, 196–204.
22 G. J. Soleas, J. Yan, T. Seaver and D. M. Goldberg, Method for the gas chromatographic assay with mass selective detection of trichloro compounds in corks and wines applied to elucidate the potential cause of cork taint, *J. Agric. Food Chem.*, 2002, **50**, 1032–1039.
23 L. Cappellin, F. D. Lopez-Hilfiker, V. Pospisilova, L. Ciotti, P. Pastore, M. Gonin and M. A. Hutterli, Thermal Desorption-Vocus Enables Online Nondestructive Quantification of 2,4,6-Trichloroanisole in Cork Stoppers below the Perception Threshold, *Anal. Chem.*, 2020, **92**, 9823–9829.
24 A. M. Peres, P. Freitas, L. G. Dias, M. E. B. C. Sousa, L. M. Castro and A. C. A. Veloso, Cyclic voltammetry: A tool to quantify 2,4,6-trichloroanisole in aqueous samples from cork planks boiling industrial process, *Talanta*, 2013, **117**, 438–444.
25 E. Moore, M. Pravda and G. G. Guilbault, Development of a biosensor for the quantitative detection of 2,4,6-trichloroanisole using screen printed electrodes, *Anal. Chim. Acta*, 2003, **484**, 15–24.
26 M. V. Duarte, P. Lozano-Sanchez and I. Katakis, Copper UPD as non-specific adsorption barrier in electrochemical displacement immunosensors, *Biosens. Bioelectron.*, 2009, **24**, 2205–2210.
27 V. Varelas, N. Sanvicens, M. Pilar-Marco and S. Kintzios, Development of a cellular biosensor for the detection of 2,4,6-trichloroanisole (TCA), *Talanta*, 2011, **84**, 936–940.
28 J. Pereira-Da-Silva, R. Rodrigues, J. Ramos, C. Brígido, A. Botnari, M. Silvestre, J. Ameixa, M. Mendes, F. Zappa, S. J. Mullock, J. M. M. Araújo, M. T. D. N. Varella, L. M. Cornetta and F. F. Da Silva, Electron Driven Reactions in Tetrafluoroethane: Positive and Negative Ion Formation, *J. Am. Soc. Mass Spectrom.*, 2021, **32**, 1459–1468.
29 G. H. Wannier, The threshold law for single ionization of atoms or ions by electrons, *Phys. Rev.*, 1953, **90**, 817–825.
30 K. M. Weitzel, J. Mähnert and M. Penno, ZEKE-PEPICO investigations of dissociation energies in ionic reactions, *Chem. Phys. Lett.*, 1994, **224**, 371–380.
31 Y.-K. Kim and M. E. Rudd, Binary-encounter-dipole model for electron-impact ionization, *Phys. Rev. A: At., Mol., Opt. Phys.*, 1994, **50**, 3954–3967.
32 W. von Niessen, J. Schirmer and L. S. Cederbaum, Computational methods for the one-particle green's function, *Comput. Phys. Rep.*, 1984, **1**, 57–125.
33 L. A. Curtiss, K. Raghavachari and J. A. Pople, Gaussian-2 theory using reduced Mo/ller – Plesset orders, *J. Am. Chem. Soc.*, 1993, **98**, 1293.
34 M. J. Frisch, G. W. Trucks, H. B. Schlegel, G. E. Scuseria, M. A. Robb, J. R. Cheeseman, G. Scalmani, V. Barone, G. A. Petersson, H. Nakatsuji, X. Li, M. Caricato, A. V. Marenich, J. Bloino, B. G. Janesko, R. Gomperts, B. Mennucci, H. P. Hratchian, J. V. Ortiz, A. F. Izmaylov, J. L. Sonnenberg, D. Williams-Young, F. Ding, F. Lipparini, F. Egidi, J. Goings, B. Peng, A. Petrone, T. Henderson, D. Ranasinghe, V. G. Zakrzewski, J. Gao, N. Rega, G. Zheng, W. Liang, M. Hada, M. Ehara, K. Toyota, R. Fukuda, J. Hasegawa, M. Ishida, T. Nakajima, Y. Honda, O. Kitao, H. Nakai, T. Vreven, K.

 This journal is © the Owner Societies 2023

Published on 29 August 2023. Downloaded on 11/29/2025 8:01:51 PM.

Throssell, J. Montgomery, J. A. J. E. Peralta, F. Ogliaro, M. J. Bearpark, J. J. Heyd, E. N. Brothers, K. N. Kudin, V. N. Staroverov, T. A. Keith, R. Kobayashi, J. Normand, K. Raghavachari, A. P. Rendell, J. C. Burant, S. S. Iyengar, J. Tomasi, M. Cossi, J. M. Millam, M. Klene, C. Adamo, R. Cammi, J. W. Ochterski, R. L. Martin, K. Morokuma, O. Farkas and J. B. Foresman, *Gaussian 16, Revision C.01*, 2016.

35 V. S. Thimmakondu and A. Karton, The quest for the carbene bent-pentadiynylidene isomer of C5H2, *Chem. Phys.*, 2018, **515**, 411–417.